ELSEVIER

Physics Letters B 541 (2002) 52–58

PHYSICS LETTERS B

www.elsevier.com/locate/npe

Low-lying dipole strength in ^{20}O

E. Tryggestad [a,b], T. Aumann [a,1], T. Baumann [a], D. Bazin [a], J.R. Beene [c], Y. Blumenfeld [a,3], B.A. Brown [a,b], M. Chartier [a,c,2], M.L. Halbert [d], P. Heckman [a,b], J.F. Liang [e], D.C. Radford [c], D. Shapira [c], M. Thoennessen [a,b], R.L. Varner [c]

[a] *National Superconducting Cyclotron Laboratory, East Lansing, MI 48824-1321, USA*
[b] *Department of Physics & Astronomy, Michigan State University, East Lansing, MI 48824-1321, USA*
[c] *Physics Division, Oak Ridge National Laboratory, PO Box 2008, Oak Ridge, TN 37831-6368, USA*
[d] *University of Tennessee, Department of Physics and Astronomy, Knoxville, TN 37996, USA*
[e] *Oak Ridge Associated Universities, Oak Ridge, TN 37831-6368, USA*

Received 21 March 2002; received in revised form 19 June 2002; accepted 28 June 2002

Editor: J.P. Schiffer

Abstract

Two 1^- levels at 5.35(10) and 6.85(5) MeV were observed for the first time in ^{20}O. The strong direct excitation and subsequent γ-ray decay of these states in virtual photon scattering at 100 MeV/nucleon, along with $B(E\lambda)$ predictions for ^{20}O states in this energy region, established their dipole character. The extracted $B(E1)\uparrow$ values of $\simeq 0.062(16)$ e^2 fm^2 and $\simeq 0.035(9)$ e^2 fm^2 for the 5.35 and 6.85 MeV states, respectively, are significantly larger than shell model calculations predict. Such large dipole strengths are not observed for low-lying 1^- states in ^{18}O, indicating a shift of dipole strength towards lower energies as one approaches the neutron drip-line.

Keywords: Coulomb excitation of ^{18}O; Coulomb excitation of ^{20}O; Virtual photon scattering on ^{18}O; Virtual photon scattering on ^{20}O; 1^- levels of ^{20}O

The changes associated with increasing proton–neutron asymmetry give rise to changes in the underlying shell structure for neutron-rich nuclei. For example, a significant amount of Giant Dipole Resonance (GDR) strength is predicted to shift to lower-lying dipole (E1) excitations due to the existence of a valence-neutron skin. The low-energy (particle-bound) part of the E1 strength distribution can then be explained as a collective vibration of the skin versus the residual nuclear core. This Pygmy resonance [1] has been observed in several heavier nuclei [2]. Similarly, in very light nuclei the existence of neutron halos [3] should lead to low lying E1 strength sometimes called the *soft* dipole resonance. Pronounced low-energy E1 transition strength has been found in several neutron-rich light nuclei [3].

E-mail address: tryggestad@nscl.msu.edu (E. Tryggestad).

[1] Present address: Gesellschaft für Schwerionenforschung, Planckstr. 1, 64291 Darmstadt, Germany.

[2] Present address: University of Liverpool, Department of Physics, Oliver Lodge Laboratory, Oxford Street, Liverpool L69 72E, UK.

[3] Present address: Institut de Physique Nucléaire, IN_2P_3-CNRS, 91406 Orsay Cedex, France.

0370-2693/02/$ – see front matter
PII: S0370-2693(02)02224-4

Being closed-shell nuclei, the oxygen isotopes are of particular interest. For example, a relativistic Coulomb excitation experiment was performed recently at GSI to study the E1 strength function of the ^{20,22,24}O isotopes above the neutron binding threshold [4]. Low-lying discrete states in ^{20}O have been probed mainly via transfer reactions with stable beams [5]. More recently, fragmentation and radioactive-beam studies have investigated the structure of ^{20}O and ^{22}O by exciting the 2_1^+ and 3_1^- states [6–8]. However, no bound 1^- states, to date, have been identified in ^{20}O.

In this Letter we report on an intermediate-energy Coulomb excitation experiment to investigate the discrete 1^- level structure of neutron-rich ^{20}O and determine the transition strengths of observed states. The motivation for such a study was to examine whether ^{20}O exhibits the predicted behavior of shifted E1 strength favoring lower-lying excitations [9,10]. In order to establish the viability of our set-up, we first performed a measurement of virtual photon scattering on stable ^{18}O.

The experiments were carried out at the National Superconducting Cyclotron Laboratory (NSCL) at Michigan State University. For the first study, ^{18}O, having been accelerated in the K1200 superconducting cyclotron to an energy of 100 MeV/nucleon, was delivered directly to the target. For the radioactive beam experiment, primary ^{22}Ne was accelerated in the K1200 to an energy of 120 MeV/nucleon. This beam impinged on a thick ^{9}Be production target. Fragments produced via projectile fragmentation were then analyzed with the A1200 fragment separator [11]. Using its combination of two magnetic bends along with a wedge energy degrader and momentum slits, this device was adjusted to select 100 MeV/nucleon ^{20}O with a momentum spread ($\Delta p/p$) of 0.5% and a purity of $\sim 85\%$.

The ^{18,20}O projectiles impinged on a 30 mg/cm^2 enriched ^{208}Pb target. Resulting reaction products were analyzed using the S800 spectrograph which was placed at 0° with respect to the beam axis. The available intensity of the ^{18}O beam ($\sim 2.5 \times 10^9$ part./s) was experimentally constrained given the capabilities of the S800 focal plane detectors [12], which can count up to $\sim 10^4$ reaction products per second. The ^{20}O intensity was limited by the secondary-beam production process to $\sim 5 \times 10^5$ part./s. The S800 focal plane detection arrangement allowed for unambiguous fragment identification (in both Z and A). The kinetic energies of identified ^{18,20}O fragments were calculated from position and trajectory information at the focus using the ion optics code COSY INFINITY [13]. S800 energy resolution of approximately 1 part in 7000 (1σ) for both experiments was achieved carrying these COSY reconstruction calculations to second order.

Gamma rays in coincidence with reaction fragments were detected using the large ORNL-TAMU-MSU BaF_2 array (144 individual elements in this configuration) which was positioned 45 cm downstream from the target and tightly packed around the beam pipe in a concentric arrangement. These γ-ray events were identified using both flight time and pulse-shape information [14,15]. Overall, the settings of the BaF_2 array for both experiments were identical with the exception of an adjustment made to the BaF_2 energy thresholds—the thresholds were lowered for the case of ^{20}O because the background counting rate was reduced given the significantly lower secondary-beam intensity.

To improve the photo-peak detection efficiency for individual γ rays, the raw BaF_2 data was processed using a shower reconstruction routine which analyzed the hit patterns and energy distributions for events with multiplicity $N > 1$. The segmentation of the array allowed for a determination of the γ-ray emission angle with respect to the scattered projectile, which facilitated a Doppler correction for individual γ-ray energies. The average energy resolution (FWHM) of the BaF_2 detectors was $\sim 8.2\%$ at 4.44 MeV [15] during the ^{20}O run.

Final event selection involved the application of simultaneous energy constraints on S800 and BaF_2 information. Specifically, it was required that the projectile energy-loss be well-correlated with the total, reconstructed γ-ray energy in the laboratory frame, as shown in Fig. 1. The enhancement of events appearing along the diagonal (dashed line) results from a concentration of events for which the detected γ-ray energy is equal to the projectile energy-loss. This final energy constraint included events where the de-excitation process proceeded through an intermediate state and one (or more) of the emitted γ rays was not detected. The resulting γ-ray spectra for ^{18}O and ^{20}O are shown in Fig. 2. Pronounced peaks observed at ~ 2 and ~ 1.7 MeV for ^{18}O and ^{20}O, re-

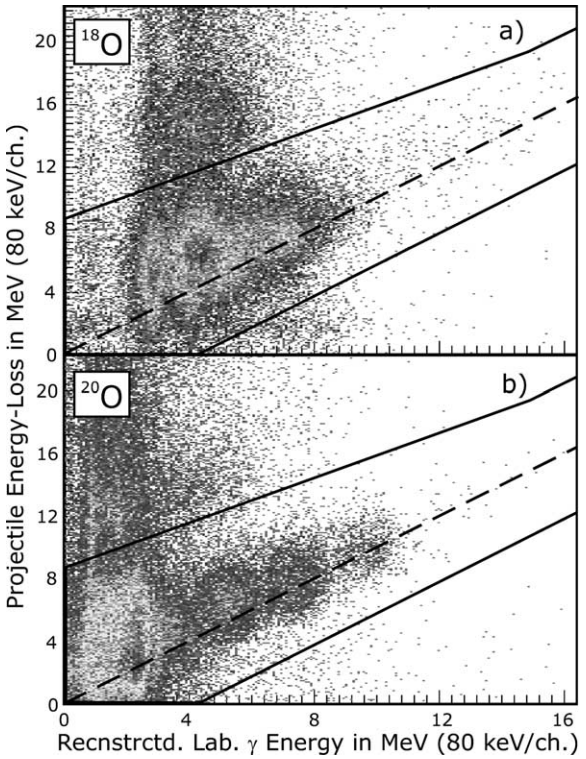

Fig. 1. ^{18}O (a) and ^{20}O (b) energy-loss as measured at the S800 focus as a function of coincident γ-ray energy. The indicated gate selects γ-ray decays back to the ground-state.

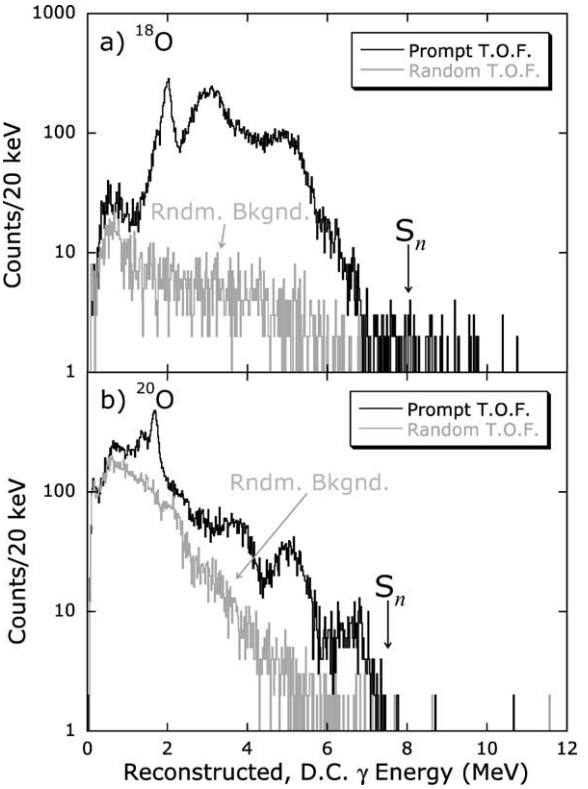

Fig. 2. ^{18}O (a) and ^{20}O (b) prompt γ-ray and background spectra extracted via time-of-flight (T.O.F.) gating.

spectively, correspond to the known 2_1^+ energies (1.98 and 1.67 MeV [5,16]), providing experimental verification of correct fragment identification and of the Doppler correction process. The figure also shows the featureless background spectra which results from random coincidence between the scattered projectiles and γ rays (or low-energy neutrons, which cannot be suppressed by pulse-shape discrimination).

In order to analyze the data and extract quantitative information about the population and decay of the observed states, a Monte Carlo simulation was developed. The simulation included the intermediate-energy Coulomb excitation formalism of Alder and Winther [17] for inelastic excitations in the projectile as well as in the target. The simulations were limited to electric virtual excitations having multipolarities $\lambda = 1, 2, 3$. Higher-multipole electric and magnetic excitations are significantly weaker and therefore were not considered. The angular acceptance for scattered projectiles ($\sim 1^\circ$ in the lab-frame) was small so that nuclear processes were negligible. The γ-ray analysis was performed by the detector simulation code GEANT [18]. The energies of the simulated γ rays were folded with the experimental BaF_2 resolution. Similarly, the known S800 resolution for measuring the energies and trajectories of scattered projectiles was incorporated. Hence, acceptance cuts similar to those that were used to constrain the experimental data could be placed on these simulated events.

Fig. 3 shows the final experimental ^{18}O γ-ray spectrum (diamonds) along with the results of the simulation (solid line) on a logarithmic scale. The spectrum is dominated at low energies by the excitation and decay of the ^{18}O first-excited 2^+ state at 1.98 MeV. The broad peak at ~ 3 MeV is a convolution of primarily two components, namely the decay remnant for de-excitations of the 2_3^+ state which have proceeded through the 2_1^+ level, and de-excitations from the 2_1^+ configuration in ^{208}Pb at 4.09 MeV (the latter contri-

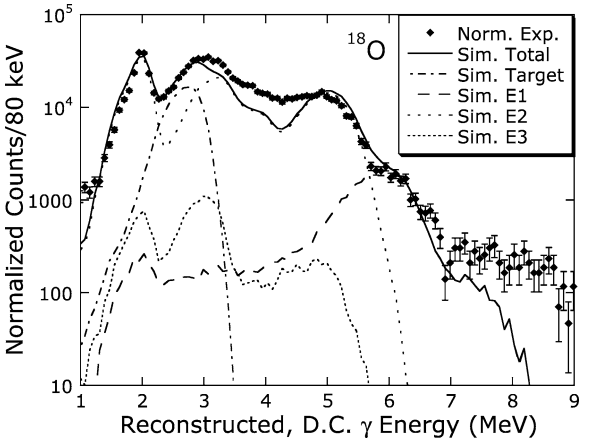

Fig. 3. Final ^{18}O experimental γ-ray spectrum (diamonds) shown with the simulated equivalent (solid line). The normalization is arbitrary. The error bars included with the experimental data are purely statistical. The individual components which contribute to the simulated strength function, namely projectile E1, E2, E3 and target background, are also shown.

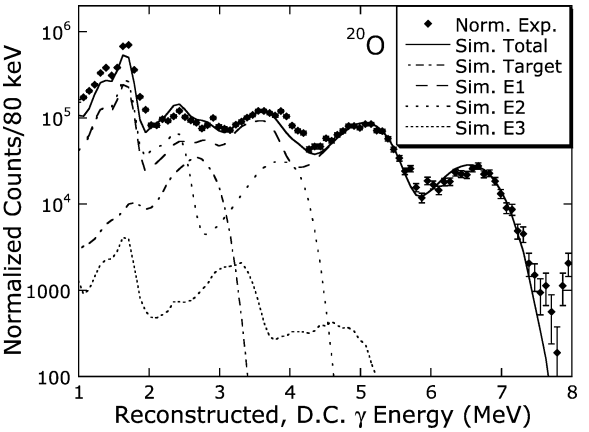

Fig. 4. Same as Fig. 3 for ^{20}O.

bution has been shifted to ~ 2.7 MeV following the Doppler correction).

These assignments were deduced from the simulation which is based on the known level schemes of the projectile (^{18}O) and target (^{208}Pb) and which included the energy, transition probability and the γ-ray branching ratios for these states [16,19–22]. Overall, the result from the simulation describes the experimental data well, with the exception of the region between ~ 3 and 4.5 MeV, where it fails to account for the full intensity in the measured spectrum. The individual contributions from target excitations and the different multipolarities of the projectile excitations are also shown in Fig. 3. The spectrum is clearly dominated by projectile E2 excitations, while target contributions cannot be neglected.

The experimental results are normalized arbitrarily to the simulated data between 2.3 and 2.9 MeV. Due to several experimental factors it was not possible to extract an absolute normalization. First, a beam-blocker was used to stop elastically-scattered beam projectiles before reaching the S800 focus. This blocker strongly influenced the acceptance of the low-energy excitations as a function of the projectile scattering angle in a complicated way. Also affecting the sensitivity to lower-energy excitations were the BaF_2 threshold settings. Variations in the fast-light output [23] of individual BaF_2 detectors (the component used for logic triggering) resulted in different threshold settings which further influenced the relative sensitivity for lower-energy γ-rays [15].

The final ^{20}O γ-ray spectrum is shown in Fig. 4 on a logarithmic scale (diamonds). Again, a dominant feature is the excitation and decay of the 2_1^+ state in the projectile at 1.67 MeV. No levels are strongly populated in the region between 2 and 5 MeV. Notice, at higher energies, approaching the neutron binding energy (7.608 MeV), two peaks are clearly visible at approximately 5.2 and 6.6 MeV. These are the same structures which appear as the two highest-energy enhancements along the diagonal in Fig. 1(b), which indicates that these excited ^{20}O configurations have strong direct ground-state decay branches.

Aside from the energies and limited spin-parity information, the only known experimental quantities are the $B(\mathrm{E2})$ value of the first-excited state and the branching ratio of the second-excited 2^+ level [5]. For the other quantities necessary to fit the γ-ray spectrum, the simulation relied on theoretical predictions. Table 1 summarizes the results of shell model calculations with different interactions. The lowest-lying positive ($J = 2$) and negative-parity ($J = 1, 3$) levels were calculated using the $1s0d$-USD [24] and the $0s$–$0p$–$1s0d$–$1p0f$-WBP [25] interaction, respectively. With regard to low-lying 1^- states, calculations which employ the $0s$–$0p$–$1s0d$–$1p0f$-WBT residual interaction [25] yield a similar result.

Fig. 4 shows the result from the ^{20}O simulation (solid line) with the normalized experimental data.

Table 1
Left panel: The pertinent ^{20}O theoretical level structure as described in the text. Right panel: The ^{20}O level scheme extracted from the fit to the experimental results presented in Fig. 4

^{20}O theory (USD/WBP)			Used for ^{20}O simulation		
E_x (MeV)	J_n^π	$B(\mathrm{E}\lambda)\uparrow$[a]	E_x (MeV)	J^π	$B(\mathrm{E}\lambda)\uparrow$[a]
2.0	2_1^+	2.9E+01	1.67[b]	2^+	3.0E+01[c]
4.2	2_2^+	7.8E+00	4.07[b]	2^+	3.0E+01
5.0	3_1^-	1.6E+03	5.00[d]	3^-	1.6E+03
5.3	2_3^+	7.0E–04	5.23[b]	2^+	7.0E–04
5.1	1_1^-	2.4E–03	5.35(10)	1^-	6.2(16)E–02
5.5	3_2^-	7.0E+02			
6.2	1_2^-	1.7E–03			
7.2	1_3^-	1.4E–03	6.85(5)	1^-	3.5(9)E–02
7.7	1_4^-	4.1E–02			
8.0	2_4^+	6.6E–01			

[a] $[B(\mathrm{E}\lambda)] = e^2\,\mathrm{fm}^{2\lambda}$.
[b] Known energy and spin-parity from Ref. [5].
[c] Known transition probability is 28(2) $e^2\,\mathrm{fm}^4$ [21].
[d] Known energy from Ref. [5], assumed to be a 3^- state.

For the reasons mentioned earlier for the ^{18}O data an absolute normalization was not possible and the data were normalized in the region between 4.5 and 8.0 MeV. The detailed composition of the γ-ray spectrum in terms of different multipolarities as well as the contribution from the target is also shown in Fig. 4.

All of the excitation parameters for this fit are listed in the right panel of Table 1. Most significant is the fact that E1 excitations dominate the strength function. This is especially true above 3 MeV. The two aforementioned peaks at ~ 5.2 MeV and ~ 6.6 MeV are identified as resulting from the γ-decay of two previously unobserved 1^- levels having energies of 5.35(10) and 6.85(5) MeV. In order to produce the observed agreement in the region between approximately 2 and 3 MeV, where the well-known target contributions are important, it was necessary to increase the $B(\mathrm{E1})$ strengths for these two 1^- levels significantly above shell model predictions for the low-lying 1^- configurations.

In addition to the excitation it is necessary to determine the branching ratios for the decay of the populated states. As previously indicated, only the branching ratios for the decay of the 2_2^+ state are known [5]. The branching probabilities used for the 3_1^- and 2_3^+ states were taken from the complimentary levels in ^{18}O. Given the fact that these states do not play an important role in the strength distribution, it is not possible to extract any quantitative information for these states. The known 0_2^+ level at 4.46 MeV [5] which is fed by the decay of the 5.35 1^- state, was assumed to decay to the ground state with 100% probability. The γ-decay branching ratios of the newly observed high-lying 1^- states which were extracted from the fit to the data presented in Fig. 4 are given in Table 2. Because of the large number of free parameters in this analysis, the estimated uncertainty of the branching ratios for the 1^- states is $\sim 20\%$.

As mentioned above, the transition strength of the E1 states had to be increased significantly compared to the shell model calculations. The 5.35 MeV state is found to have a $B(\mathrm{E1})\uparrow$ strength of $\simeq 0.062(16)\ e^2\,\mathrm{fm}^2$, which is a factor of 26 and 36 larger than the predicted WBP states at 5.1 and 6.2 MeV, respectively. Likewise, the $B(\mathrm{E1})\uparrow$ strength of the second new state is $\simeq 0.035(9)\ e^2\,\mathrm{fm}^2$, which is 20 and 25 times larger than the transition strengths for the closest predicted WBP states at 6.2 MeV and 7.2 MeV, respectively. Note, however, that the $B(\mathrm{E1})\uparrow$ for this higher-energy 1^- level agrees with the strength of the predicted state at 7.7 MeV ($B(\mathrm{E1})\uparrow = 0.041\ e^2\,\mathrm{fm}^2$). The uncertainties were estimated from a χ^2 analysis by scaling the input $B(\mathrm{E1})$ values for the

Table 2
Extracted decay branching of the two new ^{20}O 1^- states from the simulation presented in Fig. 4. The uncertainty in each decay branch is $\sim 20\%$

E_i (MeV)	$J^\pi_{n,i}$	E_f (MeV)	$J^\pi_{n,f}$	E_γ (MeV)	Br (%)
5.35	1^-_1	4.46[a]	0^+_2	0.89	19
		4.07	2^+_2	1.28	5
		1.67	2^+_1	3.68	46
		0.00	0^+_1	5.35	30
6.85	1^-_2	4.07	2^+_2	2.78	10
		1.67	2^+_1	5.18	39
		0.00	0^+_1	6.85	51

[a] Known energy and spin-parity from Ref. [5].

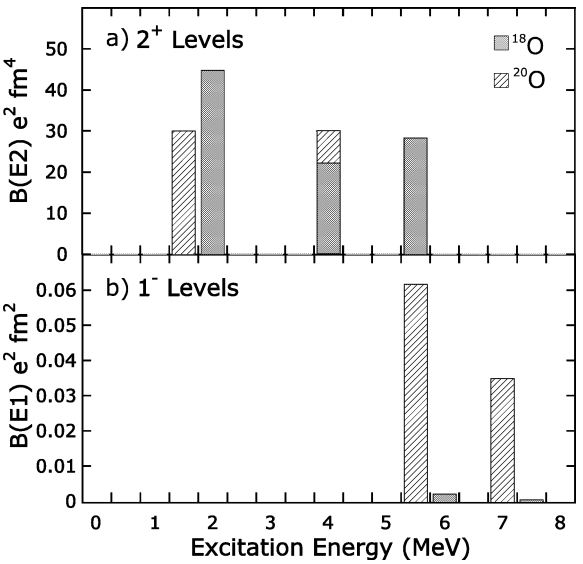

Fig. 5. A comparison of the B(E2) (a) and B(E1) (b) transition strength for ^{18}O and ^{20}O.

5.35 and 6.85 MeV states together while keeping the input branching ratios fixed.

The magnitude of the discrepancy between theory and the current results can be decreased if the p–sd shell-gap used in the calculations is reduced, which potentially reveals a manifestation of weaker neutron binding. Indeed, $0s$–$0p$–$1s0d$–$1p0f$-WBT shell model calculations [9] which have incorporated a 1.31 MeV reduction in the magnitude of p–sd shell-gap yield, for example, B(E1)↑ probabilities of 0.014 and 0.024 e^2 fm^2 for predicted 1^- states at 6.8 and 7.5 MeV [26].

It is interesting to compare the shapes of the ^{20}O and the ^{18}O spectrum. The E2 transition strength is similar for both nuclei as demonstrated in Fig. 5, which compares the B(E2) (a) and B(E1) (b) strengths extracted from the ^{18}O and ^{20}O simulations. The main difference is the high lying E1 states in ^{20}O, which are not present in ^{18}O. These states dominate not only the region above 5 MeV but the whole spectrum because of the decay branching to lower lying states.

The present data are complementary to the recent GDR measurements above the particle threshold [4]. In addition to the GDR these total photoneutron cross section results show a narrow peak near 7.8 MeV. It can be speculated that this state corresponds to the calculated 1^- state at 7.7 MeV, while the two 1^- states observed in the present experiment correspond to the 6.2 and 7.2 MeV states (given in Table 1).

It is also interesting to note that the in-beam γ-spectrum of ^{20}O following the fragmentation of ^{36}S shows similar features as the present Coulomb excitation experiment. The BaF_2 γ-ray spectrum reported in Ref. [8] reveals a structure near 5 MeV which agrees well with our identified 1^- state at 5.35 MeV. However, since the fragmentation reaction is not strongly selective with respect to the multipolarity of the states this bump may also result from excitation of the known 2^+_3 at 5.23 MeV. In addition, the low-energy portion of the broad peak observed at ~ 3.7 MeV is likely the remnant for decays from this aforementioned state above 5 MeV through the first-excited state. The high-energy portion of this broad (3.7 MeV) peak and the shoulder at ~ 2.4 MeV could be due to contributions resulting from the decay of the 2^+_2 at 4.07 MeV.

In conclusion, we populated excited states in ^{20}O by intermediate energy Coulomb excitation. Two new 1^- states were observed at 5.35(10) and 6.85(5) MeV. The observation of decays from these strongly-populated 1^- excitations between 5 and 7 MeV, which is not an important feature of the ^{18}O excitation function, is evidence for a significant shift of dipole strength towards lower excitation energies. The extracted transition strengths of $B(\mathrm{E1})\uparrow(5.35\ \mathrm{MeV}) \simeq 0.062(16)\ e^2\,\mathrm{fm}^2$ and $B(\mathrm{E1})\uparrow(6.85\ \mathrm{MeV}) \simeq 0.035(9)\ e^2\,\mathrm{fm}^2$ are significantly larger than the shell model calculations predict. However, better agreement with theory is obtained if the energy gap between the p and sd shells is reduced. This fact may reveal the physical mechanism for the emergence of low-lying dipole strength with increasing neutron excess.

Acknowledgements

This work has been supported by the National Science Foundation grant number PHY95-28844 and the Department of Energy under grant number DE-FG03-97ER41020/A000. Oak Ridge National Laboratory is managed by UT-Battelle, LLC, for the US Department of Energy under contract DE-AC05-00OR22725.

References

[1] R. Mohan et al., Phys. Rev. C 3 (1971) 1740.
[2] R.-D. Herzberg et al., Phys. Rev. C 60 (1999) 051307, and references therein.
[3] P.G. Hansen, A.S. Jensen, Annu. Rev. Nucl. Part. Sci. 45 (1995) 591, and references therein.
[4] A. Leistenschneider et al., Phys. Rev. Lett. 86 (2001) 5442.
[5] D.R. Tilley et al., Nucl. Phys. A 636 (1998) 1.
[6] P.G. Thirolf et al., Phys. Lett. B 485 (2000) 16.
[7] E. Khan et al., Phys. Lett. B 490 (2000) 45.
[8] M. Belleguic et al., Nucl. Phys. A 682 (2001) 136c.
[9] H. Sagawa, T. Suzuki, Phys. Rev. 59 (1999) 3116.
[10] N.D. Dang et al., Phys. Rev. C 63 (2001) 044302.
[11] B.M. Sherrill et al., Nucl. Instrum. Methods B 70 (1992) 298.
[12] J. Yurkon et al., Nucl. Instrum. Methods A 422 (1999) 291.
[13] M. Berz et al., Phys. Rev. C 47 (1993) 537.
[14] N.P. Shaw, High Energy γ-Rays from Highly Excited Thorium, Californium, and Meitnerium, PhD Thesis, State University of New York at Stony Brook, 1999.
[15] E. Tryggestad, Low-Lying Dipole Strength in ^{20}O, PhD Thesis, Michigan State University 2001, this document is available online at http://www.nscl.msu.edu/ourlab/library/publications/thesis.php?file=Tryggestad2001_167.pdf;
E. Tryggestad et al., in preparation.
[16] D.R. Tilley et al., Nucl. Phys. A 595 (1995) 1.
[17] K. Alder, A. Winther, Electromagnetic Excitation: Theory of Coulomb Excitation with Heavy Ions, North-Holland, 1975.
[18] Application Software Group, Computing and Networks Division, GEANT—detector description and simulation tool, CERN, Geneva, Switzerland, 1993.
[19] B.E. Norum et al., Phys. Rev. C 25 (1982) 1778.
[20] D.M. Manley et al., Phys. Rev. C 43 (1991) 2147.
[21] S. Raman et al., At. Data Nucl. Data Tables 42 (1989) 1.
[22] R.H. Spear, At. Data Nucl. Data Tables 42 (1989) 55.
[23] M. Laval et al., Nucl. Instrum. Methods 206 (1983) 169.
[24] B.A. Brown, B.H. Wildenthal, Annu. Rev. Nucl. Part. Sci. 38 (1988) 29, the sd-shell energies obtained with the USD interaction can be found online at: http://www.nscl.msu.edu/~brown/sde.htm.
[25] E.K. Warburton, B.A. Brown, Phys. Rev. C 46 (1992) 923.
[26] T. Suzuki, private communications.